Distinction of the Microcrystalline Celluloses from *Eurycoma longifolia* and *Mannihot esculenta* by Two-dimensional Correlation and Second Derivative IR Spectroscopy

Maryam Husin[1]*, Abd Rashid Li[2], Salbiah Man[2], Nur Hidayatul Khamariah Zainul Abidin[2] and Hamizah Md Rasid[1]

[1]Faculty of Applied Sciences, Universiti Teknologi MARA (UiTM), 40000 Shah Alam, Selangor, Malaysia
[2]Natural Products Division, Forest Research Institute Malaysia (FRIM), 52109 Kepong, Selangor, Malaysia
*Corresponding author (e-mail: marya911@uitm.edu.my)

In this study, the distinction of three microcrystalline cellulose (MCC) samples that have been extracted from agricultural wastes was investigated. Although all of the MCC samples possess similar molecular structures, it is hard to distinguish them in terms of their physical properties. There are problems because of interfering absorption, which makes the different IR bands overlap and makes it impossible to figure out the important properties of the MCC samples. The crystallinity index (CrI) is linked to the type of hydrogen bonding in the MCC structures, and surface morphology shows that all MCC fibres have a rough, rod-like structure on their surface. The fourier transform infrared (FT-IR) spectroscopy associated with two-dimensional correlation infrared (2D-IR) spectroscopy and second derivative infrared spectroscopy was applied to investigate the distinction between the extracted MCC. The results showed that the second derivative IR spectroscopy can enhance the spectral resolutions in the 3400 to 2900 cm^{-1} range, which provides much information regarding the strength of MCC. Whereas the 2D-IR spectra demonstrated subtle distinctions in band intensities in the region of 1500 to 850 cm^{-1}, enabling the determination of the degree of intra and inter-molecular chain length between the MCC samples. These findings will contribute to the development of rapid quality control of MCC.

Keywords: Infrared spectroscopy; microcrystalline cellulose; *Eurycoma longifolia*; *Manihot esculenta*

Microcrystalline cellulose (MCC) is typically derived from the acid hydrolysis of cellulose. Crystalline cellulose is much stronger and stiffer than amorphous cellulose and cellulose itself, and it is supposed to be a better reinforcing agent than cellulose. Many studies are ongoing to find ways to use cellulose-based fibres instead of synthetic fibres as reinforcements [1]. These natural plant fibres have various advantages over synthetic fibres, including lower density, greater stiffness, and specific strength. Additionally, plant fibres have flexibility and are therefore less susceptible to fracture during processing [2]. Ilyas *et al*. [3] have pointed out that higher crystallinity indices of celluloses result in higher tensile strength of the fibres. MCC must have excellent mechanical properties to be selected as a reinforcement to improve a polymer matrix's mechanical characteristics. The main aspect that contributes to its mechanical strength and chemical inertness is the hydrogen bonding network that holds the cellulose microfibrils together.

Infrared (IR) spectroscopy has a long tradition in wood, pulp, cellulose, and lignin research. The observed spectroscopic signals are due to the absorption of infrared radiation that is specific to the functional groups of the molecule [4]. The absorption frequencies are associated with the vibrational motions of the nuclei of the functional groups. It is extremely rapid and is a non-destructive, non-expensive, and non-invasive method for analysing the structure of wood constituents. The first use of infrared spectroscopy was to elucidate molecular structures, but some efforts have been devoted to separating the overlapping bands derived, especially from OH bands [5]. Two-dimensional correlation infrared spectroscopy (2D-IR) that has been established by Noda [6] can enhance the spectral resolution and obtain new information that cannot be acquired from the FT-IR and second derivative spectra. It is also a useful tool for studying changes in the hydrogen bonding network of cellulose under various physicochemical conditions [7].

In this study, we report on Synchronous 2D-IR correlation spectra (2D-IR *syn*) to facilitate the analytical work instead of asynchronous 2D-IR correlation spectra (2D-IR *asyn*) because, according to Noda [6], the presence of cross-peaks of 2D-IR *syn* suggests the possibility of the existence of inter- or intermolecular interactions among functional groups. Thus, the cross-peaks in 2D-IR can map out the selective correlation among IR bands in a certain way [6]. Moreover, the 2D-IR *syn* recognises the similarity

543   Maryam Husin, Abd Rashid Li, Salbiah Man,
Nur Hidayatul Khamariah Zainul Abidin
and Hamizah Md Rasid

Distinction of the Microcrystalline Celluloses from *Eurycoma longifolia* and *Mannihot esculenta* by Two-dimensional Correlation and Second Derivative IR Spectroscopy

between the variations in spectral intensities to a perturbation [8].

Although second two-dimensional correlation (2D) and derivative IR spectroscopy are useful techniques for structural characterisation, their application to MCC from these particular sources may not have received enough attention. *Eurycoma longifolia* and *Manihot esculenta* have not been investigated as much as other sources of MCC, like cotton or wood pulp. This creates a knowledge gap on the distinctive characteristics and possible uses of MCC made from these plants. Research that sufficiently compares MCC derived from different plant sources is mostly restricted to certain types of agricultural waste. It can be important to understand how the source material influences the characteristics of MCC. The purpose of the present study was to investigate the dissimilarity of the microcrystalline celluloses isolated from the stems and petioles of *Eurycoma longifolia* (longjack) and the stems of *Mannihot esculanta* (cassava) by two-dimensional correlation and second derivative IR spectroscopy. These parts of the mentioned plant species are considered agricultural wastes after the roots and leaves of *E. longifolia* and the tubers of *M. esculenta* were harvested as the main raw materials to produce health and food products, respectively. Subsequently, infrared (IR) spectrometry, x-ray diffraction (XRD), and field emission scanning electron microscopy (FESEM) were used in this recent study to determine the distinctions between the MCC samples.

EXPERIMENTAL

Plant Material

Stems (ES) and leaf petioles (EP) of *Eurycoma longifolia* (longjack) were collected at Stesen Penyelidikan FRIM, Maran, Pahang, Malaysia. Meanwhile, stems (CS) of *Manihot esculenta* (cassava) were collected at Temerloh, Pahang, Malaysia. The samples were dried and grinded into fine particles using a cutting mill (Fritsch Mill, Germany), then sieved through a 250-µm-diameter mesh size (Restch, Germany).

Preparation of Microcrystalline Cellulose

Alkali treatment was performed by mixing 100 g of dried ground powder with a 2% (w/v) NaOH solution at 120 ℃ for 1 h. It was conducted three times, and after each treatment, the fibre was filtered and washed with distilled water. The alkali-treated fibre was then bleached three times at 70 ℃ for 40 min by using 5% (v/v) H_2O_2. The bleached fibre was subsequently filtered, washed with distilled water, and oven-dried at 60 ℃ for 24 h. This was followed by treatment with a 2.5 M HCl solution at 70 ℃ for 2 h and agitation using an overhead stirrer at 200 rpm. The MCC samples obtained were filtered and washed

with distilled water, followed by oven-drying at 60 ℃ for 24 h. All MCC samples were designated as MCC_ES, MCC_EP, and MCC_CS.

Characterisation Methods

X-ray Diffraction Analysis

The diffraction pattern of the MCC samples was analysed using an XRD instrument (PANalytical, Netherlands) with Cu Kα radiation (1.5406 A˚) at 40 kV and 25 mA, in the range of $2\theta = 5\text{-}60°$ at a scanning rate of $0.02° \text{ s}^{-1}$. The crystallinity index (*CrI*) was calculated according to the Segal equation:

$$Crl = \frac{100\ x\ (I_{200} - I_{200})}{I_{200}}$$

where I_{200} is the diffraction intensity at $2\theta = 22\text{-}23°$; and I_{am} is the minimum diffraction intensity at $2\theta = 18\text{-}20°$.

Field Emission Scanning Electron Microscopy

The morphological features of all MCC samples were analysed using a FESEM (JSM-7600F, JEOL, Japan). A small amount of the samples was coated on carbon tape and then sputtered with platinum powder using an ion sputter coater. The images were taken at an accelerating potential of 10 kV.

FT-IR Spectroscopy, Second Derivative Spectroscopy and 2D-IR Spectroscopy

IR spectra were recorded on a Spectrum 100 Fourier transform-infrared (FT-IR) spectrometer (Perkin Elmer, CA, USA), equipped with a mid-infrared deuterated triglycine sulphate (DTGS) detector. A portable programmable temperature controller (4000 series TM High Stability Temperature Controller, Specac, Ltd.) was used in the range of 50-120 ℃.

All samples were ground and sieved with a 150-µm mesh. Exactly 2.0 mg of each sample was mixed with 100 mg of potassium bromide (KBr) powder, and the mixture was further ground and pressed into 13-mm-diameter disc. FT-IR spectra were recorded from a total of 16 scans in the 4000–450 cm^{-1} range with a resolution of 4 cm^{-1}. The second derivative IR spectra were obtained by using a Savitzky-Golay filter through 13-point smoothing. For the measurement of 2D-IR spectra, each sample disc was placed in the sample pool connected to a temperature controller. The dynamic 2D-IR spectra were collected at different temperatures from 50 to 120 ℃ at intervals of 10 ℃. The 2D-IR correlation spectra were acquired by treating the series of temperature-dependent dynamic spectra with 2D-IR correlation analysis employing Softdoc software developed by Tsinghua University (Beijing, China). Each sample was analysed in triplicate.

544   Maryam Husin, Abd Rashid Li, Salbiah Man,
       Nur Hidayatul Khamariah Zainul Abidin
       and Hamizah Md Rasid

Distinction of the Microcrystalline Celluloses from *Eurycoma longifolia* and *Mannihot esculenta* by Two-dimensional Correlation and Second Derivative IR Spectroscopy

Table 1. The crystallinity index (*CrI*) of MCC_EP, MCC_ES, and MCC_CS.

Sample	MCC_EP	MCC_ES	MCC_CS
Yield (%)	28.5	54.7	43.2
Crystallinity Index (%)	65.7	43.5	46.2
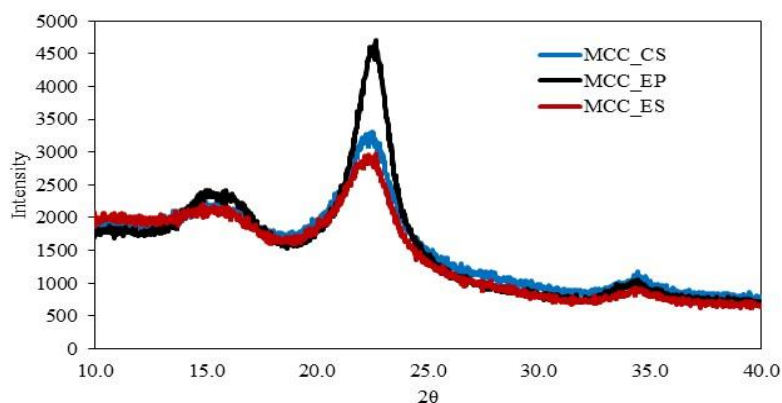
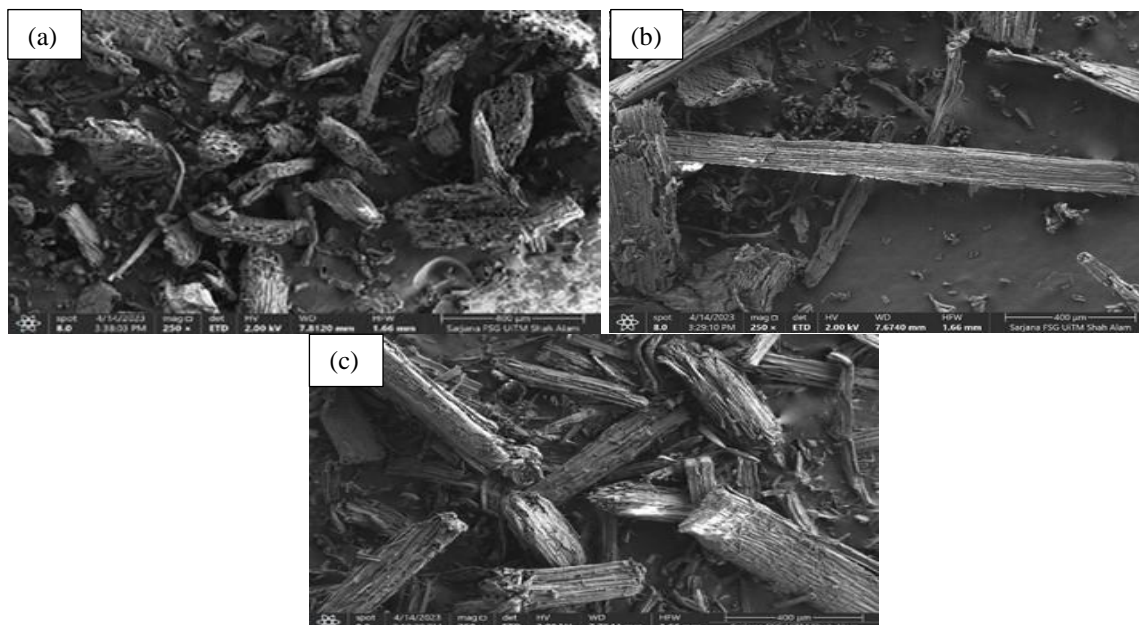**Figure 1.** Diffraction pattern of MCC_EP, MCC_ES, and MCC_CS.

RESULTS AND DISCUSSION
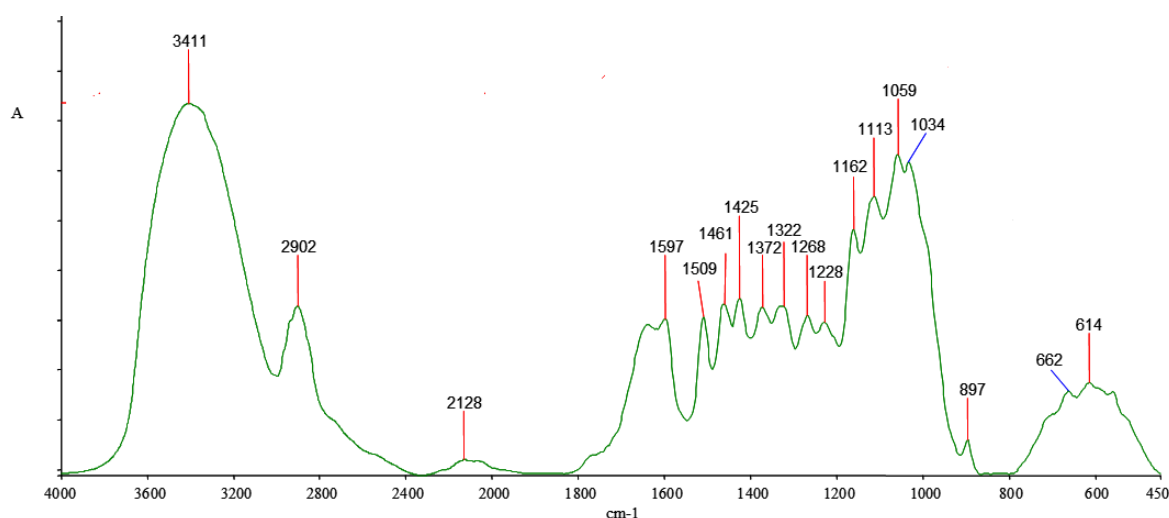
Physical Properties Analysis

The degree of crystallinity in cellulose is one of the most important characteristics contributing to its physical, chemical, and mechanical properties [9]. The crystallinity index (*CrI*) is a parameter commonly used to quantify the amount of crystalline cellulose present in cellulosic materials and has also been applied to interpret changes in cellulose structures after physicochemical and biological treatments [10]. The XRD pattern and crystallinity index of the MCC samples are displayed in Table 1 and Figure 1. Results show that the amount of crystalline cellulose in MCC_EP is higher compared to MCC_CS and MCC_ES, according to their *CrI* values. According to Ye *et al.* [11], the cellulose glucan chains are arranged in a crystalline lattice. The crystalline structure of cellulose impacts the biological processes of plants and also controls plant growth. Thus, it was expected that the difference in *CrI* in the petiole part and stem part of *E. longifolia* may be caused by the distinct crystalline lattice arrangement or orientation of glucan chains between them in their cell walls since their biological processes are different. The close *CrI* values of MCCs in the stems of *E. longifolia* and *M. esculenta* may indicate that the crystalline lattice arrangement of glucan chains in a particular part of plants is similar regardless of the plant species because they share the same biological activities. An increase in *CrI* will subsequently lead to an increase in the rigidity and stiffness of the MCC [12]. The crystallinity index (*CrI*) of MCC_EP (65.7%) is in close agreement with the *CrI* of MCC obtained from oil palm fronds (62.5%) [13]. While the *CrI* of MCC_ES (43.5%) and MCC_CS (46.2%) are in close agreement with the *CrI* of pomelo peel (40.5%) [14], they are slightly lower than the *CrI* of oil palm trunks (51.7%) [15].

Figure 2 shows the morphology of the MCC fibres of MCC_EP, MCC_ES, and MCC_CS. All MCC samples appear to have an irregular shape and a rough surface. Various factors can affect the surface morphology of Microcrystalline Cellulose (MCC) obtained from agricultural waste. These factors include the specific type of agricultural waste utilised, the procedures employed for extraction and purification, as well as any further post-treatment techniques applied. The surface imperfections and roughness revealed in the FESEM images are caused by the full elimination of lignin and hemicellulose. The lack of these cohesive elements exposes the cellulose fibres, resulting in a rougher and less uniform surface. Enhancing the surface roughness can optimise the interaction between MCC and other materials in composite applications, hence improving bonding and mechanical properties [16,17,18]. A closer examination of this micrograph revealed that the size of MCC fibres is inconsistent. Most of the MCC fibres show a rod-like structure, whereas MCC_EP possesses a longer rod structure. The variability observed in the size of those MCC fibres is due to the bundling of elementary fibres into microfibrils, which further agglomerate into macrofibrils. This reveals that all the MCC samples are free from binding particles like lignin and hemicellulose on their surfaces [19].

545   Maryam Husin, Abd Rashid Li, Salbiah Man,
       Nur Hidayatul Khamariah Zainul Abidin
       and Hamizah Md Rasid

Distinction of the Microcrystalline Celluloses from *Eurycoma longifolia* and *Mannihot esculenta* by Two-dimensional Correlation and Second Derivative IR Spectroscopy

Figure 2. FESEM Micrographs of a) MCC_ES, b) MCC_EP, and c) MCC_CS.

Figure 3. FT-IR spectra of MCC_ES with the important functional groups assigned to the frequencies/wavenumbers.

FT-IR Spectroscopy Analysis

Figure 3 shows the FT-IR spectra of MCC_ES with its important bands assigned to its related functional groups of the typical cellulosic molecular structure. It was observed that almost all the important cellulosic functional groups appear in the MCC_ES molecular structure. This was supported by the similarity of the previous FT-IR spectra with the wavenumbers of previous and recent MCC studies, as shown in Table 2.

The spectrum shows that all the samples have characteristics in common with microcrystalline cellulose (MCC), which has been reported in previous studies [4]. In addition, there is no apparent difference in terms of important cellulosic functional groups between MCC_ES, MCC_EP, and MCC_CS, as shown in Figure 4. Usually, bands at 3800-3000 cm^{-1}, 2902 cm^{-1}, 1426 cm^{-1}, 1372 cm^{-1}, and 897 cm^{-1} (Figure 3) provide information associated with the state of the crystalline and amorphous regions of the MCC [20]. According to Akerholm et al. [21], the band at around 1420-1430 cm^{-1} is associated with the amount of the crystalline structure of cellulose, while the band at 898 cm^{-1} is assigned to the amorphous region in cellulose. Those important bands obviously appeared on the FT-IR spectrum of the MCC_ES, MCC_EP, and MCC_CS samples.

546   Maryam Husin, Abd Rashid Li, Salbiah Man,
      Nur Hidayatul Khamariah Zainul Abidin
      and Hamizah Md Rasid

Distinction of the Microcrystalline Celluloses from *Eurycoma
longifolia* and *Mannihot esculenta* by Two-dimensional
Correlation and Second Derivative IR Spectroscopy

Table 2. Tabularised values of wavenumber attributed to the functional groups of MCC samples.

Wavenumber [cm^{-1}]				Functional Group
Literature [Cichosz & Masek, 2020]	MCC_EP	MCC_ES	MCC_CS	
3333	3412	3412	3349	OH (stretching) covalent bond; hydrogen bonding
2894	2904	2902	2901	CH (stretching)
1641	1636	1636	1636	Absorbed water (hydrogen-bonded)
1428	1426	1425	1427	CH$_2$ (symmetric bending)
1372	1372	1372	1372	CH (bending)
1315	1322	1322	1322	CH$_2$ (wagging) at C-6
1236	1228	1228	1228	COH (bending) in plane at C-6
1160	1161	1162	1162	COC (stretching) at β-glycosidic linkage
1104	1112	1113	1113	Ring (stretching) in plane
1030	1034	1034	1033	CO (stretching) at C-6
897	897	897	897	COC (stretching) at β-glycosidic linkage
662	662	662	662	COH (bending) out of plane
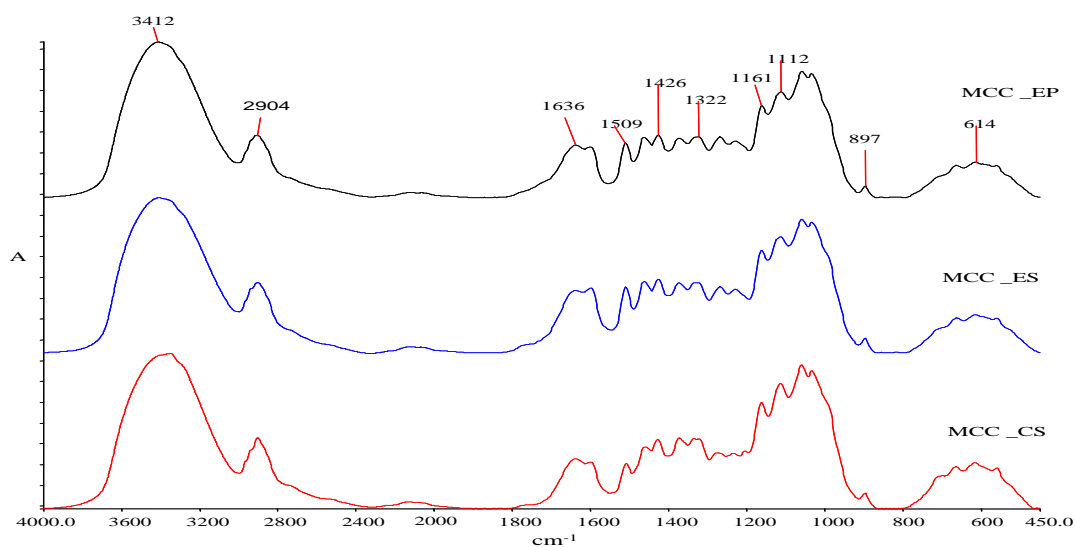
Figure 4. FT-IR spectra of overlaid spectrum of MCC_EP, MCC_ES, and MCC_CS.

Second Derivative IR Analysis

Based on the cellulose supramolecular structure point of view, which is the subject of this article, the most interesting spectrum parts are: between 3700 and 3000 cm^{-1} (where the hydrogen bond formation could be observed), from 1420 to 1430 cm^{-1} (associated with the amount of crystalline structure of the cellulose), and in the region of 900 to 890 cm^{-1} (assigned to the amorphous region). Due to the overlap of interfering bands, determining various essential characteristics of the sample, such as the wavelength, half-width, and intensity of IR absorption, becomes challenging when utilising FT-IR or 2D-IR spectroscopic techniques. To overcome those drawbacks, the second derivative IR spectroscopy approach has been recommended, as shown in Figure 5.

At the FT-IR region of 3800 to 3000 cm^{-1} (OH stretching region), MCC_ES, MCC_EP, and MCC_CS have their strongest broad bands near 3411 cm^{-1}. This region is the most interesting from a structural point of view, as the absorption bands due to OH and CH stretching vibrations are observed here. The FT-IR band at 3411 cm^{-1} as well as 2D-IR auto-peaks in the region from 3800 to 3000 cm^{-1} did not show any significant information regarding the existence of cellulose I$_\alpha$ and I$_\beta$ in the MCC samples.

547   Maryam Husin, Abd Rashid Li, Salbiah Man,
    Nur Hidayatul Khamariah Zainul Abidin
    and Hamizah Md Rasid

Distinction of the Microcrystalline Celluloses from *Eurycoma longifolia* and *Mannihot esculenta* by Two-dimensional Correlation and Second Derivative IR Spectroscopy

In nature, most cellulose occurs in the crystalline state and is defined as native cellulose I. The native cellulose I from almost all sources exists as a mixture of two crystalline forms, or polymorphs I_α and I_β. The polymorphism is most typical of crystals of organic compounds whose molecules contain groups capable of hydrogen bonding [22]. The physical properties of cellulose I_α and I_β differ from each other due to differences in their crystal packing, molecular conformation, and hydrogen bonding [23]. Cellulose I_β is more stable in chemical structure than cellulose I_α because of the intra- and intermolecular hydrogen bonding. However, when the second derivative IR technique was employed, the broad spectrum at 3411 cm^{-1} was resolved to several important peaks, especially at the frequencies of 3412, 3340, 3270, and 3233 cm^{-1} (refer to Figure 8). Those regions are very significant in providing the information associated with the ratios of polymorph I_β/I_α and lateral order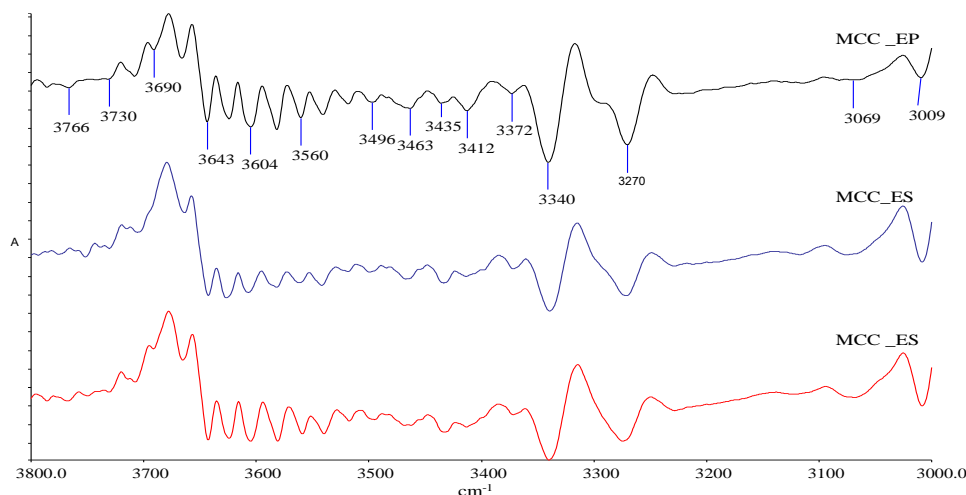 index (LOI). Both parameters are related to the crystallinity, strength, and stability of the molecular structure of the MCC.

According to Lee *et al*. [24], vibrations of cellulose I_α and I_β occur at wave frequencies of 3240 and 3270 cm^{-1}, respectively. The second derivative spectra of MCC_ES, MCC_EP, and MCC_CS in the 3800 to 3000 cm^{-1} region (Figure 6) have shown two bands at 3233 and 3270 cm^{-1}, which have been assigned to cellulose I_α and I_β, respectively.

The intensities of both bands of the MCC samples have been measured to determine the polymorph ratios of cellulose I_β to cellulose I_α (I_β/I_α) of the MCC samples (Table 3). Cellulose I_β is more stable in chemical structure than cellulose I_α. Hence, it was suggested that higher I_β/I_α values indicate the higher stability of the cellulose structure. Based on I_β/I_α, it was found that MCC_EP is more stable than MCC_CS, followed by MCC_ES.
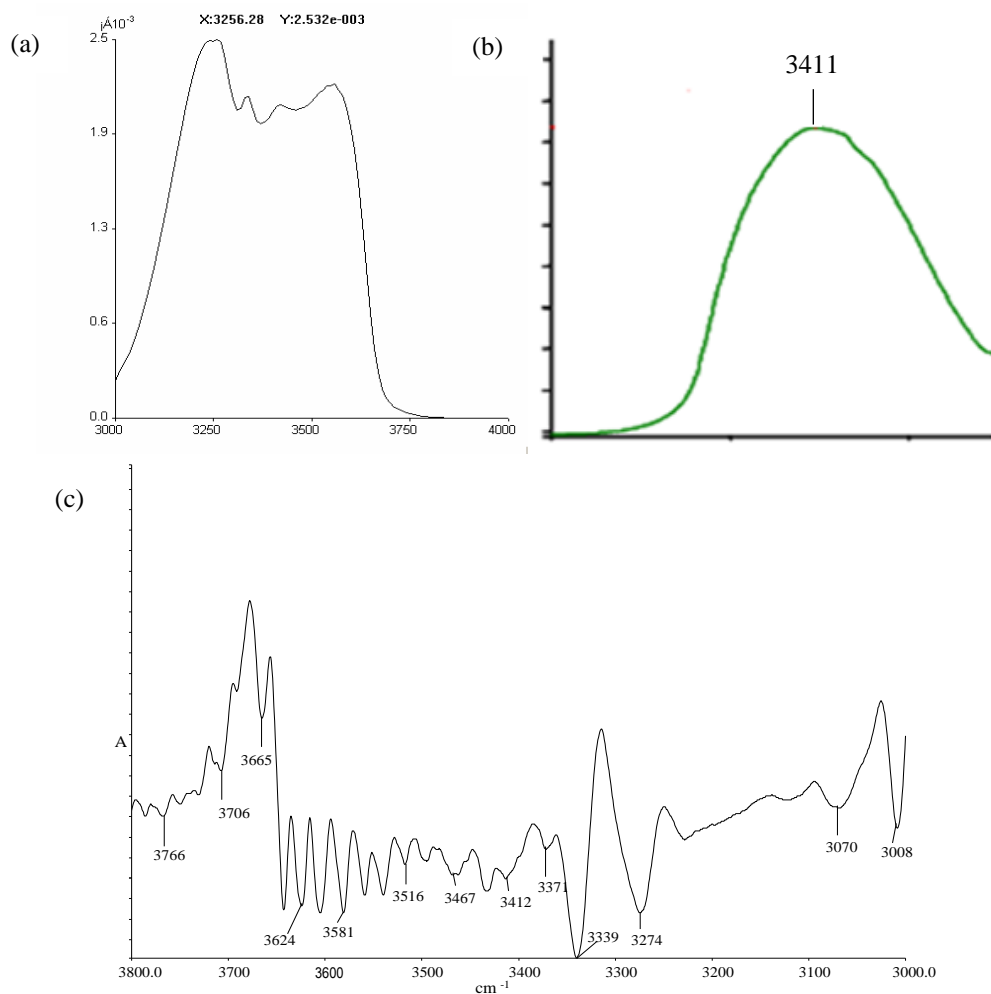
Figure 5. (a) Synchronous 2D-IR auto-peaks of MCC_ES, (b) FT-IR spectrum of MCC_ES, and (c) second derivative IR spectra of MCC_ES in the region from 3800 to 3000 cm^{-1} (peaks in the second-derivative spectra are oriented downwards).

548 Maryam Husin, Abd Rashid Li, Salbiah Man,
     Nur Hidayatul Khamariah Zainul Abidin
     and Hamizah Md Rasid

Distinction of the Microcrystalline Celluloses from *Eurycoma longifolia* and *Mannihot esculenta* by Two-dimensional Correlation and Second Derivative IR Spectroscopy

Figure 6. Second derivative IR spectrum of MCC_EP, MCC_ES, and MCC_CS in the region from 3800 to 3000 cm^{-1} (Peaks in the second-derivative spectra are oriented downwards).

Table 3. Absorbances and polymorph ratios of MCC_EP, MCC_ES, and MCC_CS.

Sample	Absorbance at 3,270 cm^{-1}	Absorbance at 3,233 cm^{-1}	I_β/I_α (A_{3270}/A_{3233})
MCC_EP	21.0	5.0	4.20
MCC_ES	14.5	4.0	3.62
MCC_CS	15.0	4.0	3.75

Cellulose microfibrils are the main structural reinforcement component of plant cell walls. It is a linear homopolysaccharide formed of 1-4 β-D-glucopyranose units, termed a glucan chain. Each D-anhydro-glucopyranose monomer bears three hydroxyl groups that can form hydrogen bonds within the same glucan chain (intra-bonding) as well as between chains (inter-bonding). These hydrogen bonds were reported to play a major role in controlling and directing (conformation) the crystalline packing as well as governing the physical properties of cellulose [25].

Between those types of hydrogen bonds, the intra-molecular O(3)H O(5) hydrogen bond is the strongest bond, which plays a great role in the rigidity of the cellulose chain, followed by other intra-molecular O(2)H (6) hydrogen bond. Meanwhile, the inter-molecular O(6)H O(3) is known as the weakest hydrogen bond type. Intra-chain H-bonds raise the stiffness of each polymer, whereas an inter-chain H-bond network links chains together to form a two-dimensional sheet [26]. In contrast, this particular sheet is mainly packed together by weak van der Waals interactions. Absorption of second-derivative spectra at 3348 to 3341 cm^{-1}, 3415 cm^{-1}, 3276 cm^{-1}, and 3233 to 3221 cm^{-1} are associated the intra-molecular O(3)H O(5), intra-molecular O(2)H O(6), inter-molecular O(6)H O(3) in cellulose I$_\beta$, and inter-molecular O(6)H O(3) in cellulose I$_\alpha$ types of hydrogen bonding, respectively [7,27].

Table 4. Tabularised values of absorbance intensities attributed to the type of hydrogen bonding in MCC samples.

Sample	Absorbance Intensities of Hydrogen Bonds			
	A_{3340} [O(3)H…O(5)]	A_{3412} [O(2)H…O(6)]	A_{3270} [O(6)H…O(3)] In cellulose I$_\beta$	A_{3233} [O(6)H…O(3)] In cellulose I$_\alpha$
MCC_EP	25.5	6.5	21.0	5.0
MCC_ES	17.5	2.0	14.5	4.0
MCC_CS	19.0	2.0	15.0	4.0

549   Maryam Husin, Abd Rashid Li, Salbiah Man,
      Nur Hidayatul Khamariah Zainul Abidin
      and Hamizah Md Rasid

Distinction of the Microcrystalline Celluloses from *Eurycoma longifolia* and *Mannihot esculenta* by Two-dimensional Correlation and Second Derivative IR Spectroscopy
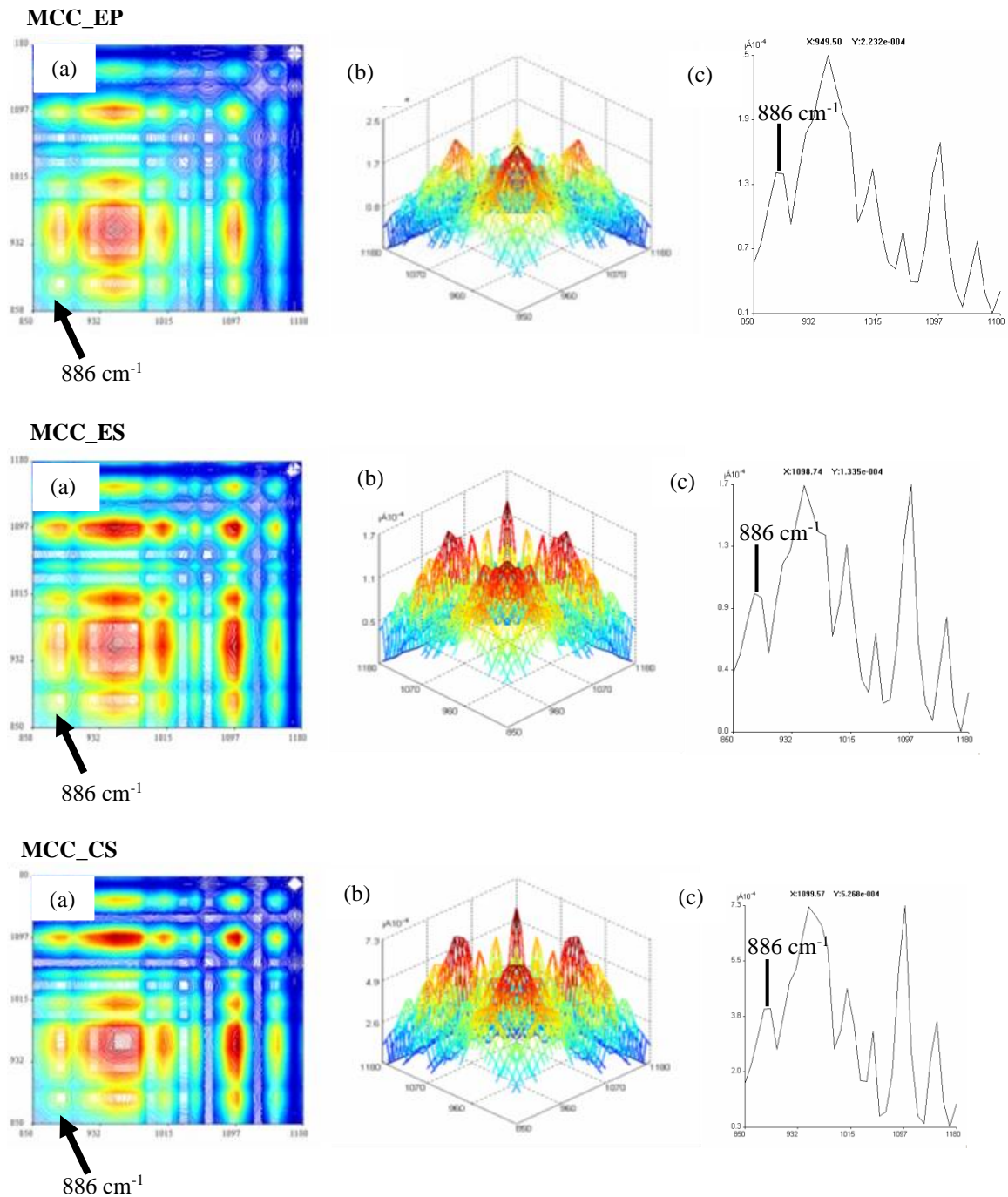
MCC_EP

MCC_ES

MCC_CS

Figure 7. Synchronous 2D-IR contour plot (a) synchronous 3D-IR mesh plot (b), a synchronous 2D-IR auto-peak curves, and (c) of MCC_ES, MCC_EP, and MCC_CS in the region from 850 to 1180 cm^{-1}.

Different band intensities at frequencies of interest for every MCC sample were observed (Table 4). This finding can be related to the concentrations or amounts of hydrogen bonds within the MCC samples. According to Chen *et al*. [28], a lower amount of hydrogen bonding between neighbouring MCC chains resulted from a less ordered cellulose structure, leading to lower *CrI* and reduced thermal stability. Thus, it was suggested that the MCC_EP is more stable compared to the MCC_CS and MCC_ES.

**Two-dimensional Correlation IR Analysis**

Two-dimensional correlation infrared spectroscopy (2D-IR) that has been established by Noda [6] can enhance the spectral resolution and obtain new information that cannot be acquired from the FT-IR and second derivative spectra. It is also a useful tool for studying changes in the hydrogen bonding network of cellulose under various physicochemical conditions [7]. The synchronous 2D-IR correlation spectrum consists of two peak types: auto-peaks and cross-peaks.

550   Maryam Husin, Abd Rashid Li, Salbiah Man,
       Nur Hidayatul Khamariah Zainul Abidin
       and Hamizah Md Rasid

Distinction of the Microcrystalline Celluloses from *Eurycoma
longifolia* and *Mannihot esculenta* by Two-dimensional
Correlation and Second Derivative IR Spectroscopy

The synchronous spectrum shows a four-way symmetric "four-leaf-clever" cluster pattern. Auto-peaks are displayed diagonally, and their intensity corresponds to the auto-correction of spectral intensity fluctuations brought on by external disturbances. The cross-peaks are offset from the diagonal and reflect the related variations in spectral intensity measured at two distinct wavenumbers. A positive cross-peak (red or green area) indicates an externally induced change in the peak intensities of two distinct groups in the same direction. In contrast, a negative cross-peak (blue area) is produced when coordinated variations in peak intensities occur in opposite directions.

The 2D-IR *syn* of the MCC_EP, MCC_ES, and MCC_CS within the range of wavenumber of 850 to 1180 cm^{-1} are shown in Figure 7. The 2D-IR *syn* of MCC_CS showed the strongest auto-peak intensity at 886 cm^{-1}, which corresponds to the absorption IR bands of COC at the β-glycosidic linkage in which the amorphous regions of MCC are located, compared to MCC_ES and MCC_EP.
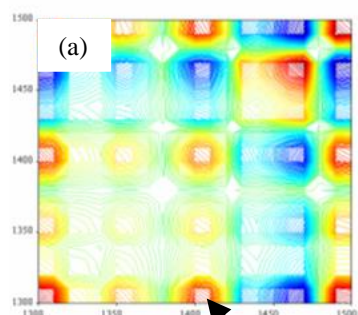
MCC_EP
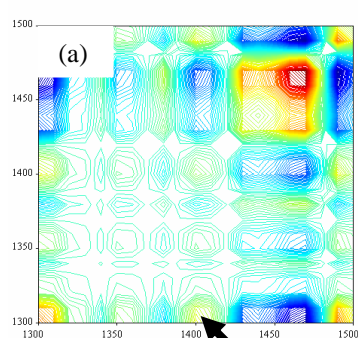
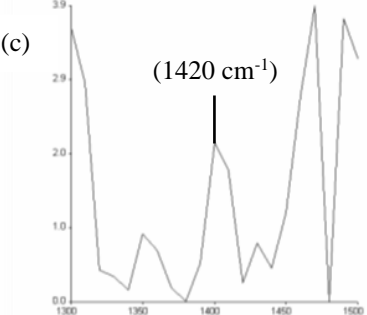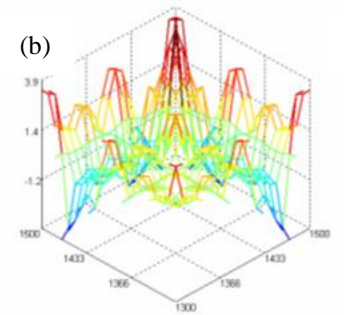(1420 cm^{-1}, 1306 cm^{-1})
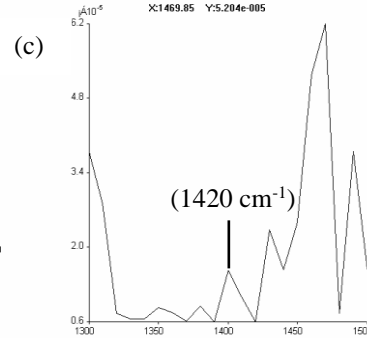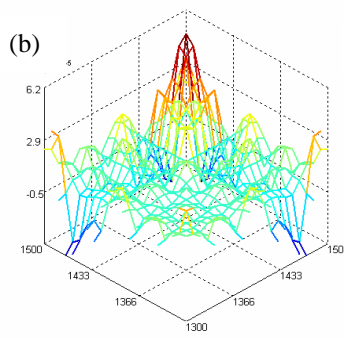
MCC_ES

(1420 cm^{-1}, 1306 cm^{-1})
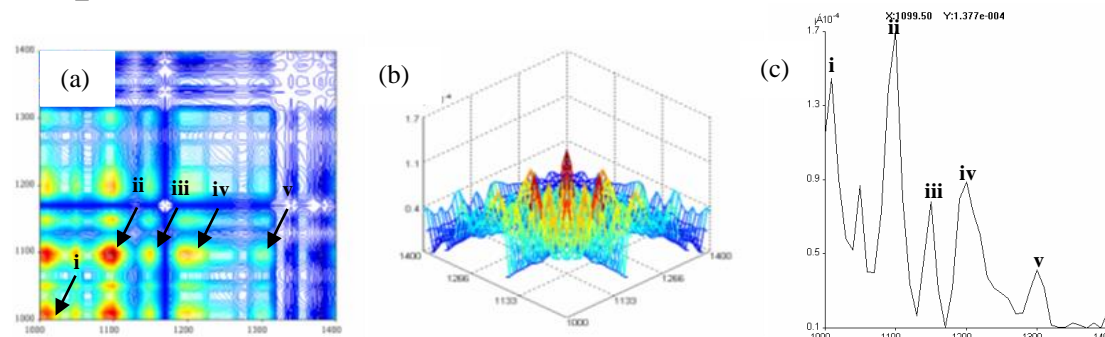
MCC_CS
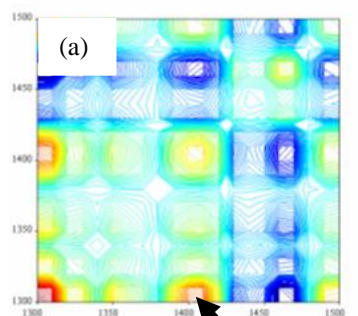
(1420 cm^{-1}, 1306 cm^{-1})
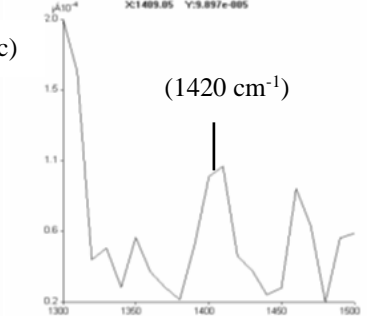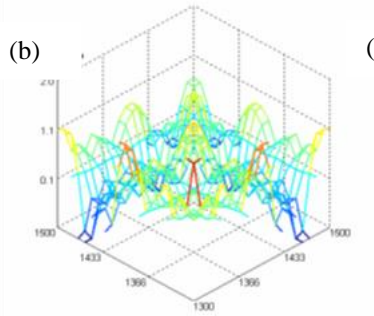
Figure 8. Synchronous 2D-IR contour plot (a), synchronous 3D-IR mesh plot (b) a synchronous 2D-IR auto-peak curves (c) of MCC_ES, MCC_EP and MCC_CS in the region from 1300 to 1500 cm^{-1}.

551   Maryam Husin, Abd Rashid Li, Salbiah Man,   Distinction of the Microcrystalline Celluloses from *Eurycoma*
      Nur Hidayatul Khamariah Zainul Abidin   *longifolia* and *Mannihot esculenta* by Two-dimensional
      and Hamizah Md Rasid   Correlation and Second Derivative IR Spectroscopy

However, within the range of 1300 to 1500 cm^{-1} (Figure 8), a strong intensity of positive cross-peak at (1420 cm^{-1}, 1306 cm^{-1}) is assigned to the absorption of the IR band of CH$_2$ (symmetric) at C-6 at 1420 cm^{-1}, where the crystalline regions were observed at 2D-IR *syn* of MCC_EP. This intensity is higher than the peak's intensities for both MCC_ES and MCC_CS. The position and intensity value of that cross-peak were determined by the correlation between contour, 3D-IR, and auto-peak curve plots. The intensity of 1420 cm^{-1} is proportional to *CrI*. Thus, it indicates that MCC_EP possesses a higher *CrI* compared to MCC_ES and MCC_CS.

Figure 9 shows that the strongest auto-peaks intensities of the MCC_CS were located at 1010 cm^{-1}

and 1100 cm^{-1} of 2D-IR *syn*, which represent the IR absorption peaks of the functional groups of CO at C-6 and alkane rings in planes, respectively. Besides that, three strong positive cross-peaks intensities located at (1152 cm^{-1}, 1100 cm^{-1}), (1204 cm^{-1}, 1100 cm^{-1}) and (1300 cm^{-1}, 1100 cm^{-1}) that corresponded to IR absorption bands of the functional groups of COH at C-6, COC of β-glycosidic linkages, and CH$_2$ at C-6, respectively, have also been observed. Based on the results, it indicates that MCC_CS has longer intra-molecular polymeric chains due to higher 2D-IR *syn* spectral intensities compared to the spectral intensities of MCC_EP and MCC_ES. The length of the intra-molecular polymeric chain of MCC is proportional to the amount of glucose alkane rings and β-glycosidic linkages.
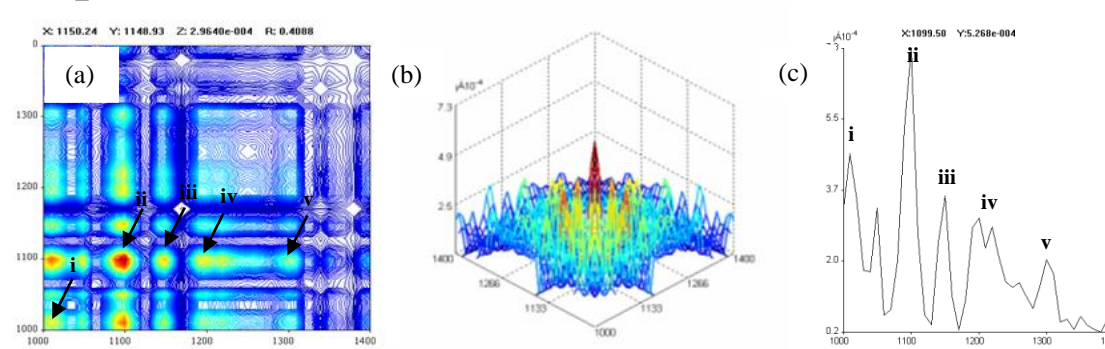
MCC_EP

MCC_ES
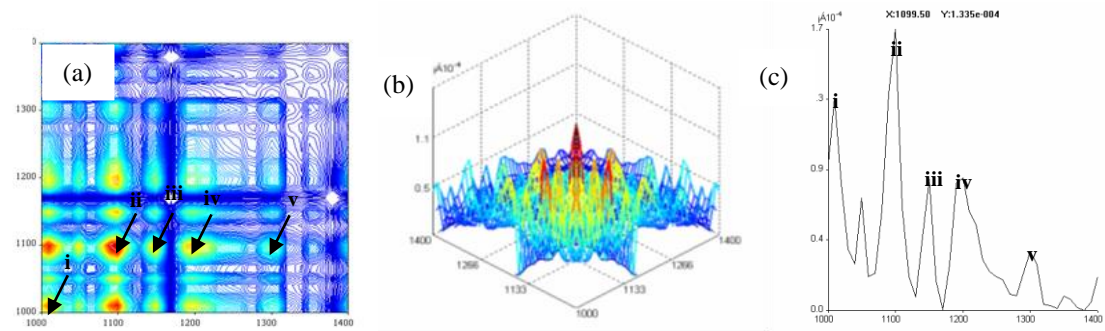
MCC_CS

Figure 9. Synchronous 2D-IR contour plot (a) synchronous 3D-IR mesh plot, (b) synchronous 2D-IR auto-peak curves, and (c) of MCC_ES, MCC_EP and MCC_CS in the region from 1,000 to 1,400 cm^{-1}. Where i) auto-peak at 1010 cm^{-1}; ii) auto-peak at 1100 cm^{-1}; iii) cross-peak at (1152 cm^{-1}, 1100 cm^{-1}); iv) cross-peak at (1204 cm^{-1}, 1100 cm^{-1}); and v) cross-peak at (1300 cm^{-1}, 1100 cm^{-1}).

552　Maryam Husin, Abd Rashid Li, Salbiah Man,
Nur Hidayatul Khamariah Zainul Abidin
and Hamizah Md Rasid

Distinction of the Microcrystalline Celluloses from *Eurycoma
longifolia* and *Mannihot esculenta* by Two-dimensional
Correlation and Second Derivative IR Spectroscopy

CONCLUSION

The present study demonstrated that second derivative IR spectroscopy and two-dimensional correlation IR (2D-IR) spectroscopy are powerful tools for analysing the complicated FT-IR spectrum of cellulose, especially in the OH stretching vibration region of the MCC. The difficulties arise due to the presence of interfering absorption, which causes overlapping of the multiple IR bands and prevents the determination of the important characteristics of the MCC samples. The capability of both IR spectroscopy techniques to resolve the overlapping IR bands has facilitated the investigation associated with the conformation of the MCC molecular structures. Combining the 2D-IR and second derivative IR methods proved that it is possible to differentiate distinct parameters between the MCC samples that have been studied. The MCC_EP, MCC_ES, and MCC_CS can be primarily discriminated according to their amount or concentrations of hydrogen bonding, crystallinity regions, and the length of the intra-molecular chains of the MCC samples. Those properties are associated with the strength and stiffness of the MCC samples, and they are very useful in determining the suitable natural-based reinforcing agents for polymer composite products. Therefore, it is recommended to apply this method to perform quality control in industries related to the production of natural-based polymers.

ACKNOWLEDGEMENTS

REFERENCES

1.　Ardanuy, M., Claramunt, J. & Toledo Filho, R. D. (2015) Cellulosic fiber reinforced cement-based composites: A review of recent research. *Construction and Building Materials*, **79**, 115–128.

2.　Li, M., Pu, Y., Thomas, V. M., Yoo, C. G., Ozcan, S., Deng, Y. & Ragauskas, A. J. (2020) Recent advancements of plant-based natural fiber–reinforced composites and their applications. *Composites Part B: Engineering*, **200**, 108254.

3.　Ilyas, R. A., Sapuan, S. M. & Ishak, M. R. (2018) Isolation and characterization of nanocrystalline cellulose from sugar palm fibres (Arenga Pinnata). *Carbohydrate Polymers*, **181**, 1038–1051.

4.　Cichosz, S. & Masek, A. (2020) IR study on cellulose with the varied moisture contents: Insight into the supramolecular structure. *Materials*, **13**(**20**), 4573.

5.　Popescu, C. M., Singurel, G., Popescu, M. C., Vasile, C., Argyropoulos, D. S. & Willför, S. (2009) Vibrational spectroscopy and X-ray diffraction methods to establish the differences between hardwood and softwood. *Carbohydrate Polymers*, **77**(**4**), 851–857.

6.　Noda I. (1990) Two-dimensional infrared (2D IR) spectroscopy: Theory and applications. *Applied Spectroscopy*, **44**(**4**), 550–561.

7.　Hishikawa, Y., Togawa, E. & Kondo, T. (2017) Characterization of individual hydrogen bonds in crystalline regenerated cellulose using resolved polarized FTIR spectra. *ACS omega*, **2**(**4**), 1469–1476.

8.　Fabian, H., Mantsch, H. H. & Schultz, C. P. (1999) Two-dimensional IR correlation spectroscopy: Sequential events in the unfolding process of the λ Cro-V55 receptor protein. *Proceeding of the National Academy of Sciences of the United States of America*, **96**(**23**), 13153–13158.

9.　Salem, K. S., Kasera, N. K., Rahman, M. A., Jameel, H., Habibi, Y., Eichhorn, S. J. & Lucia, L. A. (2023) Comparison and assessment of methods for cellulose crystallinity determination. *Chemical Society Reviews*.

10.　Al-Zuhair, S. (2008) The effect of crystallinity of cellulose on the rate of reducing sugars production by heterogeneous enzymatic hydrolysis. *Bioresource Technology*, **99**(**10**), 4078–4085.

11.　Ye, D., Rongpipi, S., Kiemle, S. N., Barnes, W. J., Chaves, A. M., Zhu, C., Norman, V. A., Liebman-Pelaez, A., Hexemer, A., Toney, M. F., Roberts, A. W., Anderson, C. T., Cosgrove, D. J., Gomez, E. W. & Gomez, E. D. (2020) Preferred crystallographic orientation of cellulose in plant primary cell walls. *Nature Communications*, **11**, 4720, 1–10.

12.　Chin, K. M., Sam, S. T. & Ong, H. L. (2019) Comparative properties analysis between micro-crystalline cellulose and cellulose nanocrystals extracted from rice straw. *Malaysian Journal of Microscopy*, **15**, 146–154.

13.　Abdulwahab, O. T., Ghazali, A., Khalil, H. A., Hassan, A., Arjmandi, R., Fazita, M. N. & Haafiz, M. M. (2016) Isolation and characterization of microcrystalline cellulose from oil palm fronds using chemo-mechanical process. *Wood and Fiber Science*, **48**(**4**), 260–270.

14.　Liu, Y., Liu, A., Ibrahim, S. A., Yang, H. & Huang, W. (2018) Isolation and characterization of microcrystalline cellulose from pomelo peel. *International journal of biological macromolecules*, **111**, 717–721.

15.　Senusi, N. A., Shohaimi, N. A. M., Ab Halim, A. Z., Shukr, N. M., Razab, M. K. A. A., Mohamed,

553 Maryam Husin, Abd Rashid Li, Salbiah Man,
Nur Hidayatul Khamariah Zainul Abidin
and Hamizah Md Rasid

Distinction of the Microcrystalline Celluloses from *Eurycoma longifolia* and *Mannihot esculenta* by Two-dimensional Correlation and Second Derivative IR Spectroscopy

M. & Abdullah, N. H. (2020) Preparation & Characterization of Microcrystalline Cellulose from Agriculture Waste. In *IOP Conference Series: Earth and Environmental Science, IOP Publishing*, **596**, 1, 012035, December, 2020.

16. Torun, S. B., Tomak, E. D., Cavdar, A. D. & Mengeloglu, F. (2021) Characterization of weathered MCC/nutshell reinforced composites. *Polymer Testing*, **101**, 107290.

17. Song, W., Gu, A., Liang, G. & Yuan, L. (2011) Effect of the surface roughness on interfacial properties of carbon fibers reinforced epoxy resin composites. *Applied surface science*, **257**(**9**), 4069–4074.

18. Sun, Z., Luo, Y., Chen, C., Dong, Z., Jiang, G., Chen, F. & Ma, P. (2023) Mechanical enhancement of carbon fiber-reinforced polymers: from interfacial regulating strategies to advanced processing technologies. *Progress in Materials Science*, **101221**.

19. Chandra, J., George, N. & Narayanankutty, S. K. (2016) Isolation and characterization of cellulose nanofibrils from arecanut husk fibre. *Carbohydrate polymers*, **142**, 158–166.

20. Oh, S. Y., Yoo, D. I., Shin, Y. & Seo G. (2005) FTIR analysis of cellulose treated with sodium hydroxide and carbon dioxide. *Carbohydrate Research*, **340**, 417-428.

21. Akerholm, M., Hinterstoisser, B. & Salmen, L. (2004) Characterization of the crystalline structure of cellulose using static and dynamic FT-IR spectroscopy. *Carbohydrate Research*, **339**, 569–578.

22. Bernstein, J. (2002) Polymorphism in Molecular Crystals Joel Bernstein. *Oxford University Press, New York*. ISBN 0198506058.

23. Fawcett, T. G., Crowder, C. E., Kabekkodu, S. N., Needham, F., Kaduk, J. A., Blanton, T. N. & Shpanchenko, R. (2013) Reference materials for the study of polymorphism and crystallinity in cellulosic. *Powder Diffraction*, **28**(**1**), 18–31.

24. Lee, C. M., Mohamed, N. M., Watts, H. D., Kubicki, J. D. & Kim, S. H. (2013) Sum-frequency-generation vibration spectroscopy and density functional theory calculations with dispersion corrections (DFT-D2) for cellulose Iα and Iβ. *The Journal of Physical Chemistry B*, **117**(**22**), 6681–6692.

25. Wohlert, M., Benselfelt, T., Wågberg, L., Furó, I., Berglund, L. A. & Wohlert, J. (2022) Cellulose and the role of hydrogen bonds: not in charge of everything. *Cellulose*, 1–23.

26. Shen, T. & Gnanakaran, S. (2009) The stability of cellulose: a statistical perspective from a coarse-grained model of hydrogen-bond networks. *Biophysical Journal*, **96**(**8**), 3032–3040.

27. Lee, C. M., Kubicki, J. D., Fan, B., Zhong, L., Jarvis, M. C. & Kim, S. H. (2015) Hydrogen-bonding network and OH stretch vibration of cellulose: Comparison of computational modeling with polarized IR and SFG spectra. *The Journal of Physical Chemistry B*, **119**(**49**), 15138–15149.

28. Chen, Q., Endo, T. & Wang, Q. (2016) Characterization of microcrystalline cellulose after pretreatment with low concentrations of ionic liquid-H_2O for a pyrolysis process. *BioResources*, **11**(**1**), 159–173.